The covariance matrix transformation method in all-earth integrated navigation considering coordinate frame conversion

OPEN ACCESS
IOP Publishing
Measurement Science and Technology
Meas. Sci. Technol. **33** (2022) 065101 (13pp)
https://doi.org/10.1088/1361-6501/ac4b11

The covariance matrix transformation method in all-earth integrated navigation considering coordinate frame conversion

Yongjian Zhang, Hui Luo, Xudong Yu, Guo Wei, Chunfeng Gao and Lin Wang*

National University of Defense Technology, College of Advanced Interdisciplinary Studies, Changsha, People's Republic of China

E-mail: wanglin11@nudt.edu.cn

Received 3 September 2021, revised 22 December 2021
Accepted for publication 13 January 2022
Published 25 February 2022

Abstract

In the exploration of polar regions, navigation is one of the most important issues to be resolved. To avoid the limitations of a single navigation coordinate frame, navigation systems usually use different navigation coordinate frames in polar and nonpolar regions, such as the north-oriented geographic frame and the grid frame. However, the error states and covariance matrix are related to the definition of the navigation coordinate frame, since coordinate frame conversion will cause overshoot of the integrated navigation Kalman filter and error discontinuity. To solve this problem, the transformation relationship of error states defined in different frames is deduced, whereby the covariance matrix transformation relationship is also analyzed. On this basis, covariance transformation-based open-loop and closed-loop Kalman filter integrated navigation algorithms are proposed. The effectiveness of the algorithms is verified by flight tests with a rotational strapdown inertial navigation system/global navigation satellite system integrated navigation system.

Keywords: covariance matrix transformation, integrated navigation, polar region, coordinate frame conversion

(Some figures may appear in color only in the online journal)

1. Introduction

With global warming and the progress of technology, the economic, political and security relations between the polar regions and countries in the rest of the world are becoming increasingly close. Exploration of the polar regions is an interest of many countries [1]. Firstly, the polar regions are rich in oil, natural gas, fresh water resources and biological resources, which have broad prospects for utilization. Secondly, the polar regions have important transportation value. If aviation flights adopt the great circle route that crosses the polar regions, the flight time can be greatly reduced, saving fuel. Besides, as the ice layer melts, new sea lanes may appear in the polar regions which will be of great value to shipping. Finally, the polar regions have a special geographical location. The sum of the distances between the north pole and other regions in the Northern Hemisphere is the shortest, which has unique military value. In addition, the ice in the polar regions can provide a concealed place for strategic nuclear submarines, making discovery more difficult.

* Author to whom any correspondence should be addressed.

When conducting scientific investigations in the polar regions, the first problem to be solved is navigation. Due to the multipath effect and the existence of the ionosphere, traditional global navigation satellite system (GNSS) positioning is more or less limited [2]. Inertial navigation with high autonomy and low external interference has become the first choice for solving positioning and navigation problems in polar regions [3]. However, inertial navigation has accumulated errors. In order to suppress error accumulation, inertial navigation is usually aided by other navigational systems, such as the GNSS, odometers and Doppler Velocity Logs [4–7]. The above mentioned multisensor navigation system is generally called the inertial navigation-based integrated navigation system, and is the preferred choice in polar region navigation.

Compared with nonpolar region navigation, polar navigation facestwo important issues, namely the physical singularities [8]. One is the collinearity between the gravity vector and the earth rotation vector at the pole, which has a negative impact on the alignment accuracy of inertial navigation systems. Some technologies have addressed this problem, such as rotation modulation-based multiposition alignment, dynamic base alignment and multisensor assistance alignment [9–11]. This problem has been well solved to some extent. The other is the rapid convergence of the meridians as the latitude increases, which makes the local-level geographic frame lose efficacy in the polar region. Namely, the traditional north-oriented heading reference loses its meaning. In order to solve this problem and find a new heading reference, the earth-centered earth-fixed (ECEF) frame [12, 13], wander frame, transversal frame [14] and grid frame [15, 16] are often used in the polar region. However, the above mentioned navigation coordinate frames also have their respective limitations. The ECEF frame can be used for continuous worldwide navigation. But its height channel is coupled with three rectangular coordinates, which causes positional errors to diverge rapidly and brings difficulties for damping filtering. Therefore, ECEF coordinate system navigation relies on external observation for correction, which is not conducive to the stability and autonomy of polar navigation. In addition, the heading reference definition of the ECEF frame is unintuitive. In fact, all the nonlocal-level navigation coordinate frames have the above mentioned limitations. The wander frame can realize global navigation, but it has the problem of wander angle failure at the poles. The transversal frame and grid frame are suitable for polar navigation, but they have singularities near the equator. In general, they cannot accomplish global navigation individually. Currently, the navigation systems usually use different navigation coordinate frames in polar and nonpolar regions to achieve global navigation, such as the north-oriented geographic frame in nonpolar regions and the transversal frame or the grid frame in the polar region [16]. In other words, the navigation coordinate frame should be converted from the north-oriented geographic frame to the transversal frame or grid frame when the carrier enters the polar region. On the contrary, the navigation coordinate frame should be converted from the transversal frame or grid frame to the north-oriented geographic frame when the carrier leaves the polar region.

For Kalman filter-based integrated navigation systems, because the error states and covariance matrix are related to the definition of the navigation coordinate frame, conversion of the navigation coordinate frame will introduce additional errors to the filter state estimation. For example, the Kalman filter state estimation will appear overshot and discontinuous [8]. In its essence, the Kalman filter error state is defined in a certain coordinate frame, and it will change along with the process of navigation coordinate frame switching. Accordingly, the covariance matrix of the Kalman filter state will also change at the same time. If the covariance matrix, especially its nondiagonal elements, is not transformed to the proper frame, the filter state overshoot and error discontinuity will appear. Although some previous studies have paid attention to this issue, for example with unified all-earth navigation mechanization [8] and the indirect polar navigation method [17, 18], the current methods do not fundamentally solve the filter consistency problem caused by navigation coordinate frame conversion. The above facts present new challenges to the Kalman filter-based integrated navigation algorithm and the Kalman filter-based damping algorithm.

In order to solve this key problem, this paper proposes an all-earth integrated navigation algorithm based on covariance transformation. The proposed method is implemented in the form of an open-loop Kalman filter and a closed-loop Kalman filter, respectively. The paper is organized as follows. Firstly, we derive and establish the transformation relationship of the error state and its covariance matrix between the local-level geographic frame and the grid frame. Secondly, we design an integrated navigation filter with a stable filter state while the coordinate frame switches. Thirdly, we verify the effectiveness of the proposed method by flight tests with the airborne single-axis rotational strapdown inertial navigation system (RSINS)/GNSS integrated navigation system. Compared with previous work, the main contributions of this paper are as follows:

(a) The transformation relationship of the error state and its covariance matrix defined in different frames is deduced, whereby an all-earth integrated navigation algorithm is proposed. The proposed methodology is also applicable to other coordinate frame conversions, such as the transversal frame and the north-oriented geographic frame.
(b) The Kalman filter-based integrated navigation algorithm is implemented in the form of an open loop and a closed loop, respectively. Two forms of filter are suitable for different scenarios.
(c) With a little software adjustment, the proposed method is conducive to the existing airborne SINS upgrade.

2. Grid frame-based polar navigation mechanization

2.1. Grid mechanization

The definition of the grid reference coordinate frame is shown in figure 1. The grid plane is parallel to the Greenwich

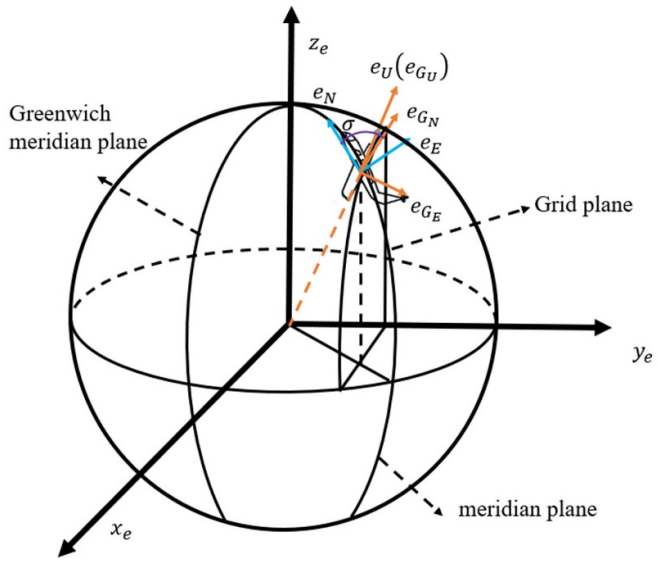

Figure 1. Grid reference frame.

meridian, and its intersection with the tangent plane at the position of the aircraft is the grid north. The angle between geographic north and grid north is the grid angle, which is clockwise as positive. The up direction of the grid frame is the same as that of the local-level geographic frame, and forms an orthogonal right-handed frame with the grid east and grid north.

The grid angle σ is expressed as [8]

$$\begin{aligned}\sin\sigma &= \frac{\sin L\sin\lambda}{\sqrt{1-\cos^2 L\sin^2\lambda}}\\ \cos\sigma &= \frac{\cos\lambda}{\sqrt{1-\cos^2 L\sin^2\lambda}}.\end{aligned} \tag{1}$$

The direction cosine matrix $\boldsymbol{C}_e^G$ between the G-frame and the e-frame (earth frame) is

$$\boldsymbol{C}_e^G = \boldsymbol{C}_n^G\boldsymbol{C}_e^n \tag{2}$$

where n refers to the local-level geographic frame. $\boldsymbol{C}_e^n$ and $\boldsymbol{C}_n^G$ are expressed as

$$\boldsymbol{C}_e^n = \begin{bmatrix} -\sin\lambda & \cos\lambda & 0\\ -\sin L\cos\lambda & -\sin L\sin\lambda & \cos L\\ \cos L\cos\lambda & \cos L\sin\lambda & \sin L\end{bmatrix}$$

$$\boldsymbol{C}_n^G = \begin{bmatrix} \cos\sigma & -\sin\sigma & 0\\ \sin\sigma & \cos\sigma & 0\\ 0 & 0 & 1\end{bmatrix}.$$

The update equations of the attitude, velocity and position in the grid frame are expressed as

$$\dot{\boldsymbol{C}}_b^G = \boldsymbol{C}_b^G\left[\boldsymbol{\omega}_{ib}^b\times\right] - \left[\boldsymbol{\omega}_{iG}^G\times\right]\boldsymbol{C}_b^G \tag{3}$$

$$\dot{\boldsymbol{v}}^G = \boldsymbol{C}_b^G\boldsymbol{f}^b - \left(2\boldsymbol{\omega}_{ie}^G + \boldsymbol{\omega}_{eG}^G\right)\times\boldsymbol{v}^G + \boldsymbol{g}^G \tag{4}$$

$$\dot{\boldsymbol{C}}_e^G = -\left[\boldsymbol{\omega}_{eG}^G\times\right]\boldsymbol{C}_e^G \tag{5}$$

$$\dot{h} = \boldsymbol{v}_U^G \tag{6}$$

where

$$\boldsymbol{\omega}_{iG}^G = \boldsymbol{\omega}_{ie}^G + \boldsymbol{\omega}_{eG}^G = \boldsymbol{C}_e^G\boldsymbol{\omega}_{ie}^e + \boldsymbol{\omega}_{eG}^G$$

$$\boldsymbol{\omega}_{ie}^G = \begin{bmatrix} -\omega_{ie}\sin\sigma\cos L\\ \omega_{ie}\cos\sigma\cos L\\ \omega_{ie}\sin L\end{bmatrix},\ \boldsymbol{\omega}_{eG}^G = \begin{bmatrix} \dfrac{1}{\tau_f} & -\dfrac{1}{R_y}\\ \dfrac{1}{R_x} & -\dfrac{1}{\tau_f}\\ \dfrac{\kappa}{\tau_f} & -\dfrac{\kappa}{R_y}\end{bmatrix}\begin{bmatrix} v_E^G\\ v_N^G\end{bmatrix}$$

and R_x is the radius of curvature of the grid east, R_y is the radius of curvature of the grid north and τ_f is the distorted radius.

The location update is implemented by updating the position matrix $\boldsymbol{C}_e^G$. The location information, for example the geographical coordinates or the rectangular coordinates, can be easily obtained through the elements of $\boldsymbol{C}_e^G$.

2.2. Dynamic model of the grid SINS

The mechanization of grid SINS is formulated in section 2.1. In order to design the Kalman filter-based integrated navigation algorithm, the system dynamic model defined in the G-frame is necessary. The three differential equations for the G-frame are given below [8].

The attitude error equation is expressed by

$$\dot{\boldsymbol{\phi}}^G = -\boldsymbol{\omega}_{iG}^G\times\boldsymbol{\phi}^G + \delta\boldsymbol{\omega}_{iG}^G - \boldsymbol{C}_b^G\delta\boldsymbol{\omega}_{ib}^b. \tag{7}$$

The velocity error equation is expressed by

$$\begin{aligned}\delta\dot{\boldsymbol{v}}^G =& \boldsymbol{f}^G\times\boldsymbol{\phi}^G + \boldsymbol{v}^G\times\left(2\delta\boldsymbol{\omega}_{ie}^G + \delta\boldsymbol{\omega}_{eG}^G\right)\\ &-\left(2\boldsymbol{\omega}_{ie}^G + \boldsymbol{\omega}_{eG}^G\right)\times\delta\boldsymbol{v}^G + \boldsymbol{C}_b^G\delta\boldsymbol{f}^b.\end{aligned} \tag{8}$$

The position error $\boldsymbol{\theta}^G$ is expressed by

$$\delta\boldsymbol{C}_e^G = -\left[\boldsymbol{\theta}^G\times\right]\boldsymbol{C}_e^G. \tag{9}$$

According to $\delta\boldsymbol{C}_e^G = \tilde{\boldsymbol{C}}_e^G - \boldsymbol{C}_e^G$ and equation (9), $\boldsymbol{\theta}^G$ can be written as

$$\begin{aligned}\boldsymbol{\theta}^G &= \begin{bmatrix}\theta_E^G & \theta_N^G & \theta_U^G\end{bmatrix}^T\\ &= \begin{bmatrix} -\cos\sigma & -\sin\sigma\\ -\sin\sigma & \cos\sigma\\ \dfrac{-\cos\sigma\sin\sigma}{\tan L} & \dfrac{-\sin^2\sigma}{\tan L}\end{bmatrix}\begin{bmatrix}\delta L\\ \delta\lambda\cos L\end{bmatrix}.\end{aligned} \tag{10}$$

The position error equation is given by

$$\dot{\boldsymbol{\theta}}^G = -\boldsymbol{\omega}_{eG}^G\times\boldsymbol{\theta}^G + \delta\boldsymbol{\omega}_{eG}^G \tag{11}$$

$$\delta\dot{h} = \delta v_U^G. \tag{12}$$

3. Covariance transformation-based integrated navigation Kalman filter algorithm

3.1. Transformation relationship of the error state and its covariance matrix between the local-level geographical frame and the grid frame

The error states of the Kalman filter are related to the navigation coordinate frame, which must be defined in a certain coordinate frame. The airborne SINS/GNSS integrated navigation system usually uses a local-level geographical frame as the navigation coordinate frame at low and middle latitudes, and uses the grid frame as the navigation coordinate frame at high latitudes. Hence, it is necessary to define proper error states in the respective frame. Once the navigation coordinate frame changes, the error state must be smoothly transformed between the different frames in addition to the navigation parameters. Note that the error state covariance matrix, especially its nondiagonal elements, is also needed to convert to the proper frame.

The error state at low and middle latitudes is expressed by

$$\begin{aligned}\boldsymbol{x}^n(t) = [&\phi_E^n, \phi_N^n, \phi_U^n, \delta v_E^n, \delta v_N^n, \delta v_U^n, \delta L, \delta\lambda, \delta h, \varepsilon_x^b, \varepsilon_y^b, \varepsilon_z^b,\\ &\times \nabla_x^b, \nabla_y^b, \nabla_{\mathrm{z}}^b]^T.\end{aligned} \tag{13}$$

At high latitudes, the integrated navigation Kalman filter is designed in the G-frame. Correspondingly, the error state should defined as

$$\begin{aligned}\boldsymbol{x}^G(t) = [&\phi_E^G, \phi_N^G, \phi_U^G, \delta v_E^G, \delta v_N^G, \delta v_U^G,\\ &\times \theta_E^G, \theta_N^G, \delta h, \varepsilon_x^b, \varepsilon_y^b, \varepsilon_z^b, \nabla_x^b, \nabla_y^b, \nabla_{\mathrm{z}}^b]^T\end{aligned} \tag{14}$$

where θ_E^G and θ_N^G are the first two components of $\boldsymbol{\theta}^G$. The third component of $\boldsymbol{\theta}^G$, i.e. θ_U^G, can be expressed by θ_E^G and θ_N^G. From equation (10), θ_U^G can be rewritten as

$$\theta_U^G = \begin{bmatrix} \dfrac{\sin\sigma}{\tan L} & 0 \end{bmatrix} \begin{bmatrix} \theta_E^G \\ \theta_N^G \end{bmatrix}. \tag{15}$$

Hence, θ_U^G does not need be a error state of the filter.

Then, the transformation relationship of the error state and the covariance matrix need to be deduced. Comparing equations (13) and (14), it can be found that the error states that remain unchanged before and after the navigation coordinate frame changes are the bias of the gyroscope $\boldsymbol{\varepsilon}^b$ and the accelerometer $\boldsymbol{\nabla}^b$. Therefore, it is sufficient to establish a transformation relationship between the attitude error $\boldsymbol{\phi}$, the velocity error $\delta\boldsymbol{v}$ and the position error $\delta\boldsymbol{p}$.

The transformation relationship between the attitude error $\boldsymbol{\phi}^n$ and $\boldsymbol{\phi}^G$ is deduced as follows:

According to the definition of $\delta\boldsymbol{C}_b^G$,

$$\delta\boldsymbol{C}_b^G = -\left[\boldsymbol{\phi}^G\times\right]\boldsymbol{C}_b^G \tag{16}$$

and from equation $\boldsymbol{C}_b^G = \boldsymbol{C}_n^G\boldsymbol{C}_b^n$, $\delta\boldsymbol{C}_b^G$ can be expressed as

$$\begin{aligned}\delta\boldsymbol{C}_b^G &= \delta\boldsymbol{C}_n^G\boldsymbol{C}_b^n + \boldsymbol{C}_n^G\delta\boldsymbol{C}_b^n\\ &= -[\boldsymbol{\phi}_{nG}^G\times]\boldsymbol{C}_n^G\boldsymbol{C}_b^n - \boldsymbol{C}_n^G[\boldsymbol{\phi}^n\times]\boldsymbol{C}_b^n\end{aligned} \tag{17}$$

where $\boldsymbol{\phi}_{nG}^G$ is the error angle vector of $\boldsymbol{C}_n^G$, which is defined as

$$\begin{aligned}\delta\boldsymbol{C}_n^G &= \tilde{\boldsymbol{C}}_n^G - \boldsymbol{C}_n^G = -\left[\boldsymbol{\phi}_{nG}^G\times\right]\boldsymbol{C}_n^G\\ \boldsymbol{\phi}_{nG}^G &= \begin{bmatrix} 0 & 0 & -\delta\sigma \end{bmatrix}^T.\end{aligned} \tag{18}$$

From equation (1), $\delta\sigma$ can be expressed as

$$\delta\sigma = \frac{\sin\sigma\cos\sigma\cos L}{\sin L}\delta L + \frac{1-\cos^2\sigma\cos^2 L}{\sin L}\delta\lambda. \tag{19}$$

Substituting for $\delta\boldsymbol{C}_b^G$ from equation (1), $\boldsymbol{\phi}^G$ can be described as

$$\boldsymbol{\phi}^G = \boldsymbol{C}_n^G\boldsymbol{\phi}^n + \boldsymbol{\phi}_{nG}^G. \tag{20}$$

The transformation relationship between the velocity error $\delta\boldsymbol{v}^n$ and $\delta\boldsymbol{v}^G$ is deduced as follows:

$$\begin{aligned}\delta\boldsymbol{v}^G &= \boldsymbol{C}_n^G\delta\boldsymbol{v}^n + \delta\boldsymbol{C}_n^G\boldsymbol{v}^n\\ &= \boldsymbol{C}_n^G\delta\boldsymbol{v}^n - \left[\boldsymbol{\phi}_{nG}^G\times\right]\boldsymbol{C}_n^G\boldsymbol{v}^n.\end{aligned} \tag{21}$$

From equation (10), the position error can be written as

$$\begin{bmatrix} \theta_E^G \\ \theta_N^G \\ \delta h \end{bmatrix} = \begin{bmatrix} -\cos\sigma & -\sin\sigma\cos L & 0 \\ -\sin\sigma & \cos\sigma\cos L & 0 \\ 0 & 0 & 1 \end{bmatrix} \begin{bmatrix} \delta L \\ \delta\lambda \\ \delta h \end{bmatrix}. \tag{22}$$

To sum up, the transformation relationship between the system error state $\boldsymbol{x}^n(t)$ and $\boldsymbol{x}^G(t)$ is as follows:

$$\boldsymbol{x}^G(t) = \boldsymbol{\Phi}\boldsymbol{x}^n(t) \tag{23}$$

where $\boldsymbol{\Phi}$ is determined by equations (20)–(22)

$$\boldsymbol{\Phi} = \begin{bmatrix} \boldsymbol{C}_n^G & \boldsymbol{O}_{3\times3} & \boldsymbol{\Phi}_a & \boldsymbol{O}_{3\times3} & \boldsymbol{O}_{3\times3} \\ \boldsymbol{O}_{3\times3} & \boldsymbol{C}_n^G & \boldsymbol{\Phi}_b & \boldsymbol{O}_{3\times3} & \boldsymbol{O}_{3\times3} \\ \boldsymbol{O}_{3\times3} & \boldsymbol{O}_{3\times3} & \boldsymbol{\Phi}_c & \boldsymbol{O}_{3\times3} & \boldsymbol{O}_{3\times3} \\ \boldsymbol{O}_{3\times3} & \boldsymbol{O}_{3\times3} & \boldsymbol{O}_{3\times3} & \boldsymbol{I}_{3\times3} & \boldsymbol{O}_{3\times3} \\ \boldsymbol{O}_{3\times3} & \boldsymbol{O}_{3\times3} & \boldsymbol{O}_{3\times3} & \boldsymbol{O}_{3\times3} & \boldsymbol{I}_{3\times3} \end{bmatrix}.$$

Table 1. Open-loop Kalman filter algorithm.

	Without covariance transformation	With covariance transformation
Initial state	$\boldsymbol{C}_b^n, \boldsymbol{v}^n, \boldsymbol{C}_e^n, h, \boldsymbol{P}^n, \boldsymbol{x}^n$	$\boldsymbol{C}_b^n, \boldsymbol{v}^n, \boldsymbol{C}_e^n, h, \boldsymbol{P}^n, \boldsymbol{x}^n$
Navigation parameter conversion	$\hat{\boldsymbol{C}}_b^G = \left(\boldsymbol{I} + \left[\boldsymbol{\phi}_{nG}^G\times\right]\right)\boldsymbol{C}_n^G\left(\boldsymbol{I} + [\boldsymbol{\phi}^n\times]\right)\boldsymbol{C}_b^n$ $\hat{\boldsymbol{v}}^G = \left(\boldsymbol{I} + \left[\boldsymbol{\phi}_{nG}^G\times\right]\right)\boldsymbol{C}_n^G\left(\boldsymbol{v}^n + \delta\boldsymbol{v}^n\right)$ $\hat{\boldsymbol{C}}_e^G = \left(\boldsymbol{I} + \left[\boldsymbol{\phi}_{nG}^G\times\right]\right)\boldsymbol{C}_n^G\left(\boldsymbol{I} + [\boldsymbol{\theta}^n\times]\right)\boldsymbol{C}_e^n$ $\hat{h} = h + \delta h$	$\boldsymbol{C}_b^G = \boldsymbol{C}_n^G\boldsymbol{C}_b^n$ $\boldsymbol{v}^G = \boldsymbol{C}_n^G\boldsymbol{v}^n$ $\boldsymbol{C}_e^G = \boldsymbol{C}_n^G\boldsymbol{C}_e^n$
Error state conversion	$\boldsymbol{x}^G = \boldsymbol{O}_{15\times1}$	$\boldsymbol{x}^G = \boldsymbol{\Phi}\boldsymbol{x}^n$
Covariance conversion	$\boldsymbol{P}^G = \boldsymbol{P}^n$	$\boldsymbol{P}^G = \boldsymbol{\Phi}\boldsymbol{P}^n\boldsymbol{\Phi}^T$

$$\boldsymbol{\Phi}_a = \frac{1}{R}\begin{bmatrix} 0 & 0 & 0 \\ 0 & 0 & 0 \\ \cos L\cos\lambda\sin\sigma\cos\sigma + \dfrac{\left(\cos^2 L\cos^2\sigma - 1\right)}{\sin L\cos L} & \cos L\sin\lambda\sin\sigma\cos\sigma - \dfrac{\left(\cos^2 L\cos^2\sigma - 1\right)}{\sin L\cos L} & \dfrac{-\cos^2 L\sin\sigma\cos\sigma}{\sin L} \end{bmatrix}$$

$$\boldsymbol{\Phi}_b = \begin{bmatrix} 0 & -v_U^G & v_N^G \\ v_U^G & 0 & -v_E^G \\ -v_N^G & v_E^G & 0 \end{bmatrix}\boldsymbol{\Phi}_a$$

$$\boldsymbol{\Phi}_c = \begin{bmatrix} -\cos\sigma & -\sin\sigma\cos L & 0 \\ -\sin\sigma & \cos\sigma\cos L & 0 \\ 0 & 0 & 1 \end{bmatrix}.$$

The transformation relationship of the covariance matrix is as follows:

$$\begin{aligned} \boldsymbol{P}^G(t) &= \boldsymbol{E}\left\{\left(\tilde{\boldsymbol{x}}^G(t) - \boldsymbol{x}^G(t)\right)\left(\tilde{\boldsymbol{x}}^G(t) - \boldsymbol{x}^G(t)\right)^{\mathrm{T}}\right\} \\ &= \boldsymbol{E}\left\{\boldsymbol{\Phi}\left(\tilde{\boldsymbol{x}}^n(t) - \boldsymbol{x}^n(t)\right)\left(\tilde{\boldsymbol{x}}^n(t) - \boldsymbol{x}^n(t)\right)^{\mathrm{T}}\boldsymbol{\Phi}^{\mathrm{T}}\right\} \\ &= \boldsymbol{\Phi}\boldsymbol{E}\left\{\left(\tilde{\boldsymbol{x}}^n(t) - \boldsymbol{x}^n(t)\right)\left(\tilde{\boldsymbol{x}}^n(t) - \boldsymbol{x}^n(t)\right)^{\mathrm{T}}\right\}\boldsymbol{\Phi}^{\mathrm{T}} \\ &= \boldsymbol{\Phi}\boldsymbol{P}^n(t)\boldsymbol{\Phi}^{\mathrm{T}}. \end{aligned} \tag{24}$$

When the aircraft flies out of the polar region, $\boldsymbol{x}^G$ and $\boldsymbol{P}^G$ are converted to $\boldsymbol{x}^n$ and $\boldsymbol{P}^n$, which can be described as

$$\begin{aligned} \boldsymbol{x}^n(t) &= \boldsymbol{\Phi}^{-1}\boldsymbol{x}^G(t) \\ \boldsymbol{P}^n(t) &= \boldsymbol{\Phi}^{-1}\boldsymbol{P}^G(t)\boldsymbol{\Phi}^{-\mathrm{T}}. \end{aligned} \tag{25}$$

3.2. Navigation coordinate frame switching process in open-loop and closed-loop Kalman filters

The Kalman filter-based integrated navigation algorithm can be implemented with the form of an open loop or a closed loop, which are applicable to different scenarios. The open-loop Kalman filter algorithm does not need corrective feedback operation, and can maintain the independence of SINS and GNSS. Hence, it can be used to improve the anti-jamming capability of polar navigation. The error state of the closed-loop Kalman filter algorithm is fed back every iteration, which can keep the Kalman filter states small, minimizing the effect of nonlinearity. The closed-loop Kalman filter is especially suitable for the low-cost SINS, for example microelectromechanical systems-based integrated navigation systems.

The open-loop Kalman filter algorithm includes a predication update and a measurement update, but it does not have feedback loop. Hence, its error state is not a zero vector and the error state updates step by step according to the system prediction model. When the navigation coordinate frame is converting, the error state must be transformed simultaneously. Otherwise, the error state estimation of an open-loop Kalman filter will present a transient overshoot, and the navigation accuracy will decrease significantly. Similarly, the covariance matrix must be also be transformed at the same time. The transformation relationships are shown by equation (23). To sum up, when the carrier enters or leaves the polar region, the error state and covariance matrix should be transformed based on the transformation matrix $\boldsymbol{\Phi}$ in addition to the well-known navigation parameters conversion process. The open-loop Kalman filter switching process from the local-level geographical frame to the grid frame is shown in the table 1. The inverse process is similar.

This paper adopts the scheme of feedback correction when covariance transformation is not used. In table 1, $\hat{\boldsymbol{C}}_b^G$, $\hat{\boldsymbol{v}}^G$, $\hat{\boldsymbol{C}}_e^G$ and $\hat{h}$ represent the attitude, velocity and position with feedback correction, respectively.

For the closed-loop Kalamn filter, the error state is a zero vector at the beginning of the navigation coordinate frame conversion due to real-time feedback. Hence, the error state

Table 2. Closed-loop Kalman filter algorithm.

	Without covariance transformation	With covariance transformation
Initial state	$\boldsymbol{C}_b^n, \boldsymbol{v}^n, \boldsymbol{C}_e^n, h, \boldsymbol{P}^n, \boldsymbol{x}^n = \boldsymbol{O}_{15\times1}$	$\boldsymbol{C}_b^n, \boldsymbol{v}^n, \boldsymbol{C}_e^n, h, \boldsymbol{P}^n, \boldsymbol{x}^n = \boldsymbol{O}_{15\times1}$
Navigation parameter conversion	$\boldsymbol{C}_b^G = \boldsymbol{C}_n^G \boldsymbol{C}_b^n$ $\boldsymbol{v}^G = \boldsymbol{C}_n^G \boldsymbol{v}^n$ $\boldsymbol{C}_e^G = \boldsymbol{C}_n^G \boldsymbol{C}_e^n$	$\boldsymbol{C}_b^G = \boldsymbol{C}_n^G \boldsymbol{C}_b^n$ $\boldsymbol{v}^G = \boldsymbol{C}_n^G \boldsymbol{v}^n$ $\boldsymbol{C}_e^G = \boldsymbol{C}_n^G \boldsymbol{C}_e^n$
Error state conversion	$\boldsymbol{x}^G = \boldsymbol{O}_{15\times1}$	$\boldsymbol{x}^G = \boldsymbol{O}_{15\times1}$
Covariance conversion	$\boldsymbol{P}^G = \boldsymbol{P}^n$	$\boldsymbol{P}^G = \boldsymbol{\Phi}\boldsymbol{P}^n\boldsymbol{\Phi}^T$

does not need to be transformed. Besides the transformation of the navigation parameters, it is only necessary to transform the covariance matrix $\boldsymbol{P}$ by the constructed transformation matrix $\boldsymbol{\Phi}$. As a contrast, during the traditional switching process, only the velocity, position and attitude are transformed to the grid frame, the covariance matrix is not transformed. Hence, the Kalman filter state estimation presents overshoot.

The closed-loop Kalman filter switching process from the local-level geographical frame to the grid frame is shown in table 2. The inverse process is similar.

4. Experimental results and discussions

To verify the effectiveness of the proposed method, flight experiments with airborne RSINS/GNSS were conducted. RSINS with a ring laser gyroscope adopts single-axis rotation modulation. The single-axis rotation around the azimuth axis can modulate the constant drift error of the gyroscope and accelerometer perpendicular to the rotation axis. Hence, it can improve navigational accuracy in long-endurance inertial navigation. The ring laser gyro bias stability is less than 0.003° h^{-1}. The accelerometer bias stability is less than 20 μg. The GNSS positioning error is less than 10 m, which is used as the position reference. The update frequency of the gyro and accelerometer is 200 Hz while the update frequency of the GNSS is 1 Hz. Experiments are carried out at 31.1° N. Firstly, multiposition alignment is used to improve alignment accuracy, and the alignment time is about 2 h. Then, the aircraft takes off, and the experimental data are saved for offline analysis. During the experiment, the navigation coordinate frame is the local-level geographic frame in the first hour. After that, the navigation coordinate frame is changed to the grid frame until the end of the flight. In this way, the scenario in which the carrier enters and leaves the polar region can be simulated.

Since the flight experiments are carried out at middle latitudes, the integrated navigation results based on the local-level geographic frame without navigation coordinate frame conversion are highly accurate, and can be used as a reference to evaluate the accuracy of the proposed method. In order to unify the comparison benchmark, all navigation parameters are transformed to the local-level geographic frame for convenience.

Table 3. Direct switching in the open-loop Kalman filter algorithm.

Initial state	$\boldsymbol{C}_b^n, \boldsymbol{v}^n, \boldsymbol{C}_e^n, \boldsymbol{P}^n, \boldsymbol{x}^n$
Navigation parameter conversion	$\boldsymbol{C}_b^G = \boldsymbol{C}_n^G \boldsymbol{C}_b^n$ $\boldsymbol{v}^G = \boldsymbol{C}_n^G \boldsymbol{v}^n$ $\boldsymbol{C}_e^G = \boldsymbol{C}_n^G \boldsymbol{C}_e^n$
Error state conversion	$\boldsymbol{x}^G = \boldsymbol{x}^n$
Covariance conversion	$\boldsymbol{P}^G = \boldsymbol{P}^n$

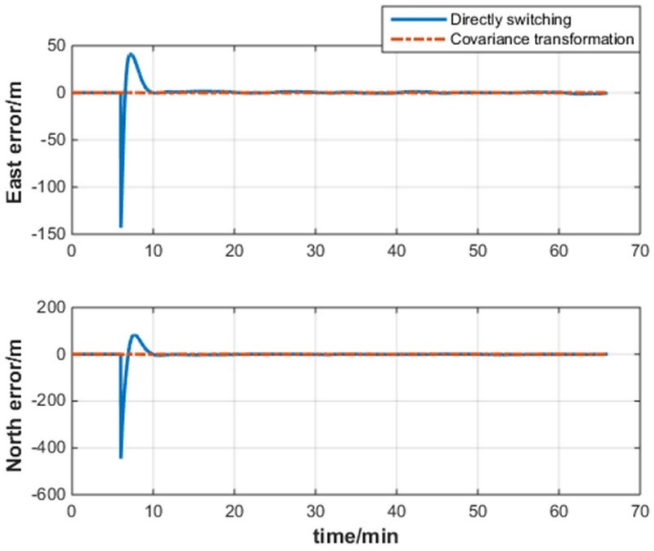

Figure 2. The relative error of position.

4.1. Flight test based on the open-loop Kalman filter

In the open-loop filter, when converting the navigation coordinate frame, the simplest way is direct switching, the process of which is shown in table 3. Unlike the conversion method mentioned in table 1, the direct conversion process has no feedback. The results of the direct switching method are compared with the results of the single north-oriented geographic frame, which are shown in figures 2–5.

As shown in figures 2–5, the direct switching method brings a great switching error. The relative position error reaches 427 m. The relative yaw error is $1.2'$. The maximum bias

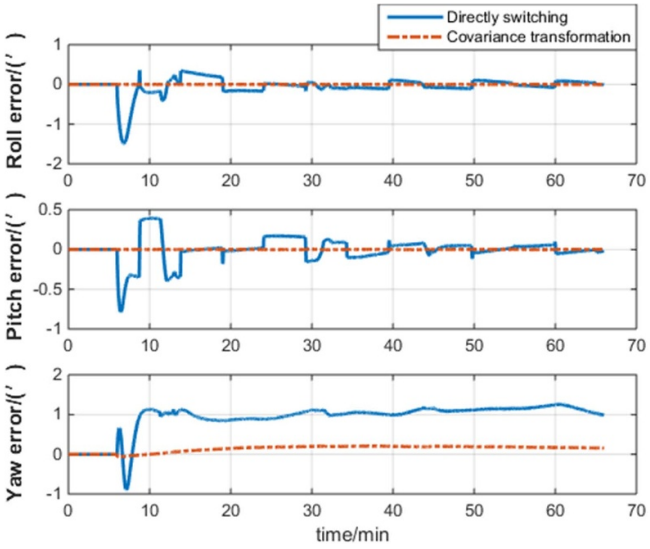

Figure 3. The relative error of attitude.

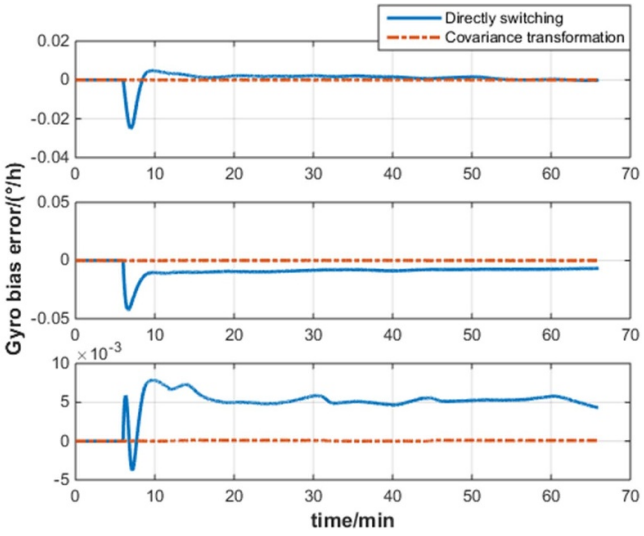

Figure 4. The relative error of gyro bias estimation.

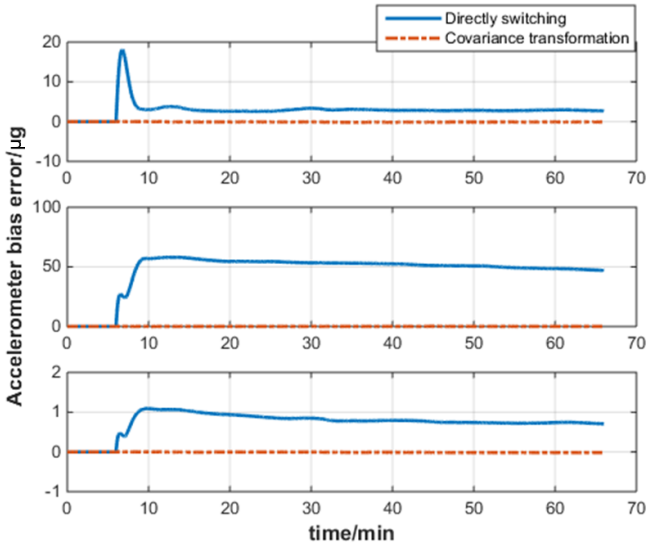

Figure 5. The relative error of accelerometer bias estimation.

error of the gyroscope and accelerometer reach 0.043° h^{-1} and 58 μg, respectively. Ignoring the difference between $\boldsymbol{x}^G$ and $\boldsymbol{x}^n$ causes great relative error. As the error state accumulates in a single coordinate frame, the switching error will become larger.

In order to ensure consistency of navigation, we adopt the scheme of feeding back the error state estimation to the navigation parameters and resetting it to zero before coordinate frame conversion, then transforming the navigation parameters to the grid frame. The process is listed in table 1. Note that the covariance matrix is not yet transformed. Compared with the scheme using covariance matrix transformation, the results are shown in figures 6–9.

As shown in figure 6, the relative position error is 0.9 m without covariance transformation. The integrated navigation result with covariance transformation shows better stability and a smaller relative position error of 0.24 m. As shown in figure 7, the relative yaw error is the largest, and reaches 1.47′ without covariance transformation. The integrated navigation result with covariance transformation had a smaller relative yaw error of 0.22′. In addition, there is a sawtooth error in the roll angle and pitch angle, which is caused by periodic rotation modulation around the azimuth. Figure 8 shows that the maximum bias error of the gyroscope with and without covariance transformation can reach 0.0004° h^{-1} and 0.013° h^{-1}, respectively. As shown in figure 9, the maximum bias error of the accelerometer with and without covariance transformation reaches 0.21 μg and 2.28 μg, respectively.

Compared with direct switching, the feedback process can reduce the error state estimation error to some extent. But the navigation results still show error fluctuations due to the neglect of transformation of the covariance matrix $\boldsymbol{P}$. As a comparison, the covariance transformation method ensures

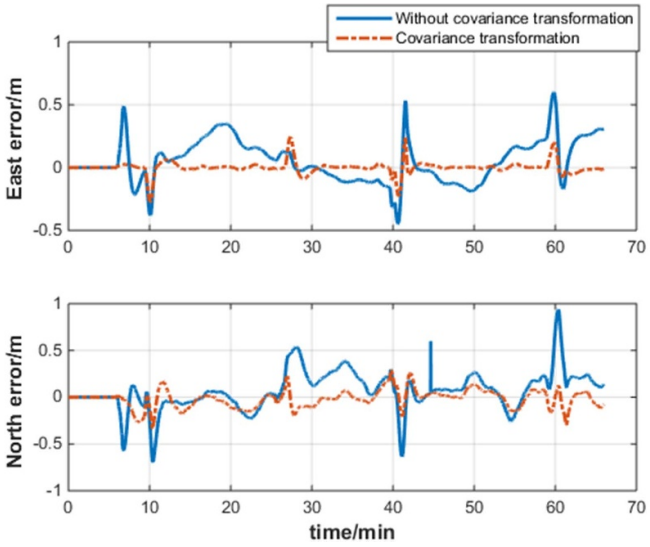

Figure 6. The relative error of position.

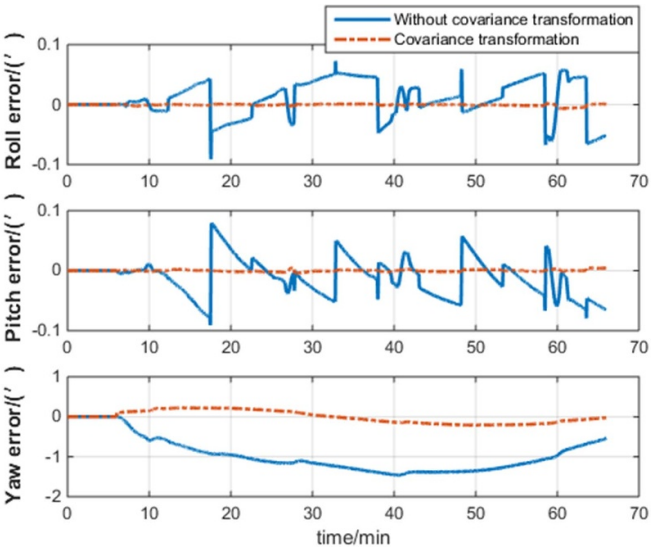

Figure 7. The relative error of attitude.

the consistency and continuity of filter state estimation before and after coordinate frame conversion, and reduces the error caused by navigation coordinate frame conversion.

In order to make our conclusion more convincing, the open-loop filter experiments were carried out six times. The root mean square (RMS) not only reflects the amplitude of the oscillation, but also relates to the time of the oscillation. The RMS of the relative error data within 1 h after navigation frame conversion is shown in tables 4 and 5.

As shown in figure 10, the relative position error is 1.8 m without covariance transformation, which is almost equal to the relative position error with covariance transformation. Due to the GNSS position and velocity being used as measurements and the real-time feedback, the covariance transformation has less effect on the reduction of relative position error. As shown in figure 11, the relative yaw error reaches 0.79′ without covariance transformation. The integrated navigation result with covariance transformation has a smaller relative yaw error of 0.28′. Figure 12 shows that the maximum bias error of the gyroscope with and without covariance transformation reaches 0.001° h^{-1} and 0.009° h^{-1}, respectively. As shown in figure 13, the maximum bias error of the accelerometer with and without covariance transformation reaches 0.67 μg and 2.34 μg, respectively.

As shown in tables 4 and 5, the covariance transformation method can reduce the error caused by conversion of the navigation coordinate frame by at least 50%.

4.2. Flight test based on the closed-loop Kalman filter

As shown in table 2, in the case of the closed-loop filter, the error state is a zero vector at the beginning of conversion of the navigation coordinate frame due to real-time feedback. It is only necessary to transform the covariance matrix P by the

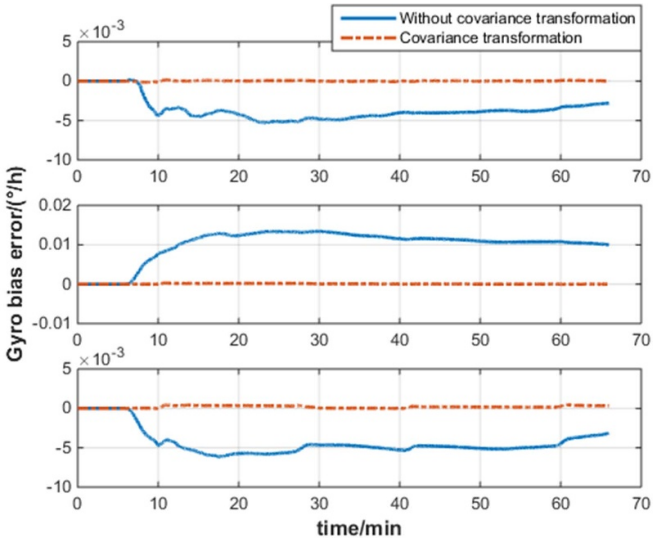

Figure 8. The relative error of gyro bias estimation.

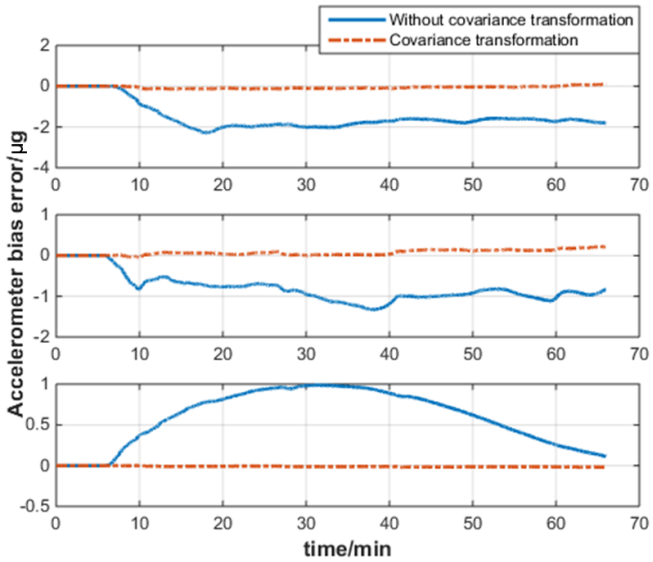

Figure 9. The relative error of accelerometer bias estimation.

Table 4. RMS of state estimation relative error with covariance transformation.

Number	Attitude error (′)	Velocity error (m s^{-1})	Position error (m)	Gyro bias error (° h^{-1})	Accelerometer bias error (μg)
1	0.16	0.004	0.12	0.00024	0.10
2	0.17	0.003	0.10	0.00008	0.10
3	0.02	0.002	0.09	0.00005	0.03
4	0.08	0.002	0.08	0.00002	0.02
5	0.04	0.001	0.06	0.00003	0.03
6	0.07	0.002	0.08	0.00003	0.05
Average	0.09	0.002	0.09	0.00008	0.05

constructed transformation matrix $\mathbf{\Phi}$. The integrated navigation results based on the local-level geographic frame without navigation coordinate frame conversion are used as reference to evaluate the accuracy of the proposed method. The relative error of the navigation results based on the closed-loop Kalman filter are shown in figures 10–13.

Consistent with the open-loop filter experiments, the closed-loop filter experiments were carried out six times. The

Table 5. RMS of state estimation error without covariance transformation.

Number	Attitude error (′)	Velocity error (m s^{-1})	Position error (m)	Gyro bias error (° h^{-1})	Accelerometer bias error (μg)
1	1.10	0.015	0.30	0.01135	1.72
2	0.26	0.005	0.14	0.00152	0.44
3	0.23	0.003	0.11	0.00218	0.19
4	0.12	0.004	0.21	0.00111	0.40
5	0.22	0.002	0.07	0.00199	0.17
6	0.24	0.002	0.09	0.00133	0.48
Average	0.36	0.005	0.15	0.00325	0.57

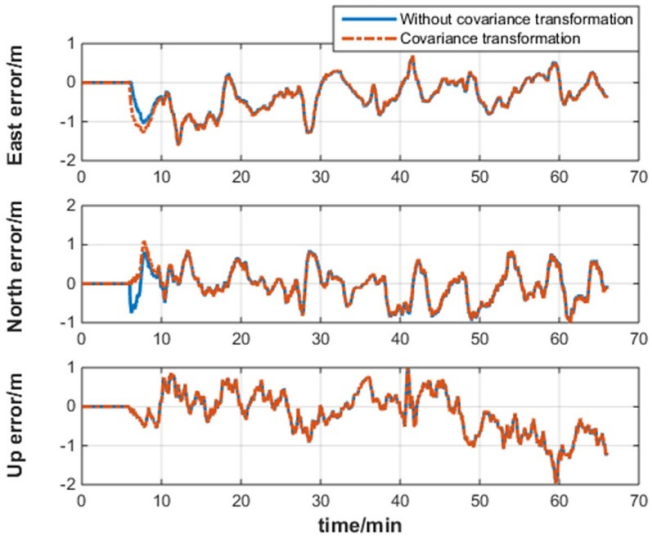

Figure 10. The relative error of position.

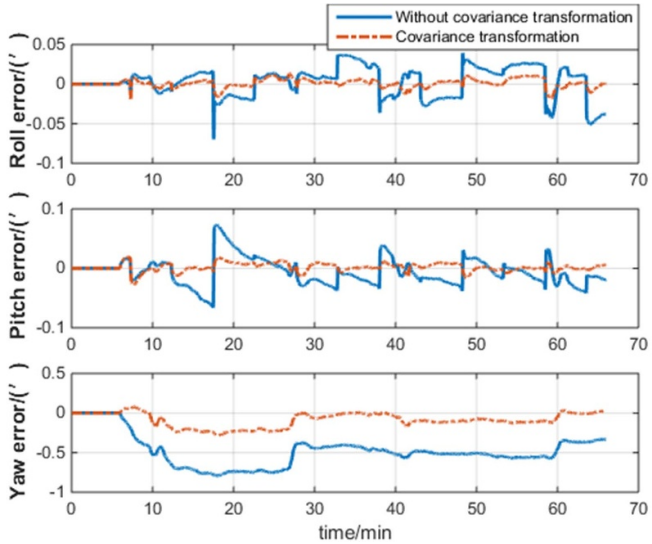

Figure 11. The relative error of attitude.

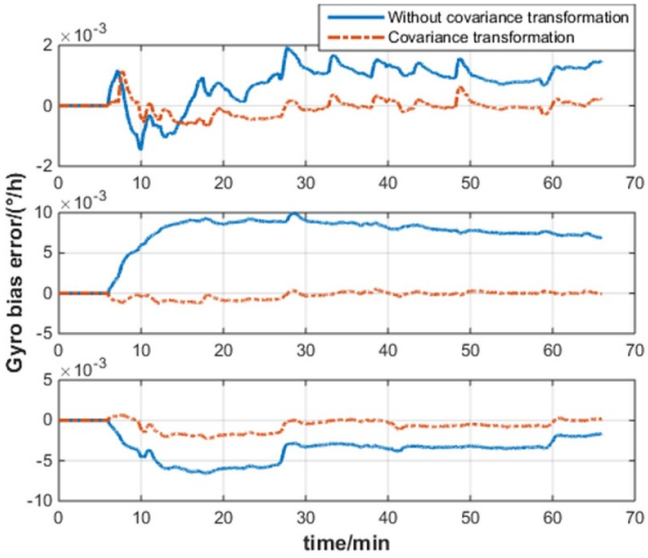

Figure 12. The relative error of gyro bias estimation.

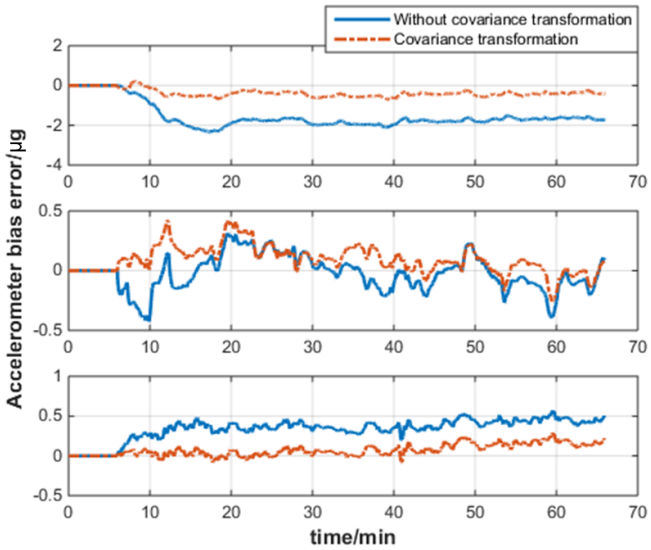

Figure 13. The relative error of accelerometer bias estimation.

Table 6. RMS of state estimation error with covariance transformation.

Number	Attitude error (′)	Velocity error (m s^{-1})	Position error (m)	Gyro bias error (° h^{-1})	Accelerometer bias error (μg)
1	0.13	0.018	0.70	0.00101	0.44
2	0.04	0.017	0.63	0.00022	0.21
3	0.05	0.018	1.11	0.00053	0.16
4	0.04	0.021	0.97	0.00036	0.20
5	0.06	0.019	0.85	0.00062	0.28
6	0.05	0.020	0.93	0.00042	0.49
Average	0.06	0.019	0.87	0.00053	0.29

Table 7. RMS of state estimation error without covariance transformation.

Number	Attitude error (′)	Velocity error (m s^{-1})	Position error (m)	Gyro bias error (° h^{-1})	Accelerometer bias error (μg)
1	0.55	0.019	0.68	0.00802	1.75
2	0.17	0.017	0.63	0.00180	0.39
3	0.21	0.018	1.12	0.00222	0.17
4	0.11	0.021	0.99	0.00102	0.33
5	0.19	0.019	0.85	0.00206	0.40
6	0.18	0.020	0.94	0.00136	0.50
Average	0.24	0.019	0.87	0.00275	0.59

statistical results of the experiments are shown in tables 6 and 7.

As shown in tables 6 and 7, except for velocity error and position error, the error caused by switching the navigation coordinate frame will be reduced by at least 50% through the covariance transformation method.

5. Conclusion

In order to solve the problem of the integrated navigation Kalman filter overshoot and error discontinuity caused by coordinate frame conversion, we proposed in this paper an all-earth integrated navigation algorithm. The proposed method takes the grid frame and the local-level geographic frame as an example to derive the transformation relationship of the error state and the covariance matrix. The Kalman filter-based integrated navigation algorithm is implemented in the form of an open loop and a closed loop. We studied the application in two situations. By comparing the results of the open-loop filter experiment and the closed-loop filter experiment, it was found that the proposed covariance transformation method can effectively reduce the state estimation error peak caused by navigation coordinate frame conversion by more than 50%. The effect is more obvious in the open-loop filter.

Generally, the covariance transformation method fundamentally solves the problem of filter overshoot and error discontinuity caused by navigation coordinate frame conversion, and improves the navigation accuracy when crossing the polar region. The proposed method only needs a small software adjustment, and hence is conducive to the existing airborne SINS upgrade. In addition, the covariance transformation method is also applicable to other coordinate frame conversions.

Data availability statement

The data that support the findings of this study are available upon reasonable request from the authors.

Acknowledgments

This work was partially funded by the National Nature Science Foundation of China under Grant No. 62003360 and the Basic Research Project of College of Advanced Interdisciplinary Studies under Grant No. ZDJC19-07. The authors would like to thank all the editors and anonymous reviewers for improving this article.

ORCID iDs

Yongjian Zhang https://orcid.org/0000-0001-9537-6745
Xudong Yu https://orcid.org/0000-0002-3082-0830

References

[1] Zhao Y, Ben Y and Li Q 2020 Inertial navigation systems for polar marine navigation: a survey *Navig. Positioning Timing* **7** 1–10
[2] Zhao B, Zeng Q, Liu J, Gao C and Zhao T 2021 A new polar alignment algorithm based on the Huber estimation filter with the aid of Beidou navigation satellite system *Int. J. Distrib. Sens. Netw.* **17** 13
[3] Xu B and Li S 2020 Rapid alignment for SINS based on expansion of observation vectors in polar regions *Optik* **206** 163151
[4] Sun J, Ma S, Wang J, Yang J and Liu M 2020 Reconciliation problem in polar integrated navigation considering coordinate frame transformation *IEEE Trans. Veh. Technol.* **69** 10375
[5] Zhao L, Kang Y, Cheng J and Wu M 2019 A fault-tolerant polar grid SINS/DVL/USBL integrated navigation algorithm based on the centralized filter and relative position measurement *Sensors* **19** 3899
[6] Song L *et al* 2019 Based on grid reference frame for SINS/CNS integrated navigation system in the polar regions *Complexity* **2019** 2164053
[7] Zhao L, Wu M, Ding J and Kang Y 2018 A joint dual-frequency GNSS/SINS deep-coupled navigation system for polar navigation *Appl. Sci.* **8** 2322
[8] Fu Q, Zhou Q, Yan G, Li S and Wu F 2021 Unified all-earth navigation mechanization and virtual polar region technology *IEEE Trans. Instrum. Meas.* **70** 8501211
[9] Cheng J, Wang T, Guan D and Li M 2016 Polar transfer alignment of shipborne SINS with a large misalignment angle *Meas. Sci. Technol.* **27** 035101
[10] Wang T, Cheng J, Guan D, Kang Y and Zhang W 2017 Modified compensation algorithm of lever-arm effect and flexural deformation for polar shipborne transfer alignment based on improved adaptive Kalman filter *Meas. Sci. Technol.* **28** 095101
[11] Wang L, Wu W, Wei G, Lian J and Yu R 2018 A polar-region-adaptable systematic bias collaborative measurement method for shipboard redundant rotational inertial navigation systems *Meas. Sci. Technol.* **29** 055106

[12] Babich O A 2019 Extension of the basic strapdown INS algorithms to solve polar navigation problems *Gyroscopy Navig.* **10** 330–8
[13] Wu Y, He C and Liu G 2020 On inertial navigation and attitude initialization in polar areas *Satell. Navig.* **1** 4
[14] Huang L, Xu X, Zhao H and Ge H 2020 Transverse SINS/DVL integrated polar navigation algorithm based on virtual sphere model *Math. Probl. Eng.* **2020** 8892750
[15] Ge H *et al* 2021 Grid SINS/GNSS integrated navigation algorithm based on the virtual sphere model in polar region *Navig. Positioning Timing* **8** 81–87
[16] Song L-J, Yang G-Q, Zhao W-L, Ding Y-J, Wu F and He X 2020 The inertial integrated navigation algorithms in the polar region *Math. Probl. Eng.* **2020** 5895847
[17] Yao Y, Xu X and Tong J 2015 Indirect transverse inertial navigation algorithm in polar region *J. Chin. Inert. Technol.* **23** 29–34
[18] Zhou Q *et al* 2014 Indirect grid inertial navigation mechanization for transpolar aircraft *J. Chin. Inert. Technol.* **22** 18–22